Chin. J. Astron. Astrophys. Vol. 3 (2003), No. 4, 316–340
(http://www.chjaa.org or http://chjaa.bao.ac.cn)

Chinese Journal of
Astronomy and
Astrophysics

Non-LTE Analysis of the Sodium Abundance of Metal-Poor Stars in the Galactic Disk and Halo*

Yoichi Takeda[1], Gang Zhao[2], Masahide Takada-Hidai[3], Yu-Qin Chen[2],
Yu-ji Saito[4] and Hua-Wei Zhang[5,6]

[1] Komazawa University, Komazawa, Setagaya, Tokyo 154-8525, Japan; takedayi@cc.nao.ac.jp
[2] National Astronomical Observatories, Chinese Academy of Sciences, Beijing 100012
[3] Liberal Arts Education Center, Tokai University, Hiratsuka, Kanagawa 259-1292, Japan
[4] Department of Physics, Faculty of Science, Tokai University, Hiratsuka, Kanagawa 259-1292, Japan
[5] Department of Astronomy, School of Physics, Peking University, Beijing 100871
[6] CAS-Peking University Joint Beijing Astrophysical Center, Beijing 100871

Received 2003 March 10; accepted 2003 March 27

Abstract We performed an extensive non-LTE analysis of the neutral sodium lines of Na I 5683/5688, 5890/5896, 6154/6161, and 8183/8195 in disk/halo stars of types F–K covering a wide metallicity range ($-4 \lesssim$ [Fe/H] $\lesssim +0.4$), using our own data as well as data collected from the literature. For comparatively metal-rich disk stars ($-1 \lesssim$ [Fe/H] $\lesssim +0.4$) where the weaker 6154/6161 lines are the best abundance indicators, we confirmed [Na/Fe] ~ 0 with an "upturn" (i.e., a shallow/broad dip around $-0.5 \lesssim$ [Fe/H] $\lesssim 0$) as already reported in previous studies. For the metal-deficient halo stars, where the much stronger 5890/5896 or 8183/8195 lines subject to considerable (negative) non-LTE corrections amounting to 0.5 dex have to be used, our analysis suggests mildly "subsolar" [Na/Fe] values down to ~ -0.4 (with a somewhat large scatter of $\sim \pm 0.2$ dex) on the average at the typical halo metallicity of [Fe/H] ~ -2, followed by a rise again to a near-solar ratio of [Na/Fe] ~ 0 at the very metal-poor regime [Fe/H] ~ -3 to -4. These results are discussed in comparison with the previous observational studies along with the theoretical predictions from the available chemical evolution models.

Key words: Galaxy: evolution — radiative transfer — stars: abundances — stars: atmospheres — stars: late-type

1 INTRODUCTION

The purpose of this paper is to clarify the behavior of the sodium abundance of disk/halo stars in our Galaxy.

* Supported by the National Natural Science Foundation of China.

Recently, we carried out an extensive non-LTE abundance analysis of potassium based on the K I 7699 resonance line and found a tendency of mildly supersolar [K/Fe] ratios for metal-poor stars just as in the case of α-capture elements (Takeda et al. 2002). As a continuation of that study, we pay attention this time to another alkali element, sodium (Na).

The main site of Na synthesis is considered to be the hydrostatic carbon burning inside massive stars (e.g., Woosley & Weaver 1995), though other manufacturing processes (e.g., Ne-Na cycle in the H-burning shell, type I supernova, etc.) are possible and may have appreciably affected its chemical history (see, e.g., Timmes et al. 1995). As an odd-Z (neutron-rich) element, its production is sensitive to neutron excess and is therefore metal-dependent. Hence, clarifying the behavior of its abundance in terms of the cosmic metallicity would provide us important information concerning the variation of the yield, the detailed mechanism of the synthesis, and the Galaxy evolution models (initial mass function, infall, etc.).

Unlike the case of potassium, a reasonable number of adequate lines are available for sodium abundance determinations; these lie mostly in the visible through near-IR wavelength regions. Hence, many observational studies have been performed over the last two decades (see, e.g., the references quoted in the recent theoretical papers such as Timmes et al. 1995, Samland 1998, and Goswami & Prantzos 2000). Nevertheless, the behavior of [Na/Fe] is currently still controversial and has not yet been settled.

It was generally considered until the mid-1990's that Na almost scales with Fe at all metallicities though with a considerable scatter around [Na/Fe] ~ 0. (See, for example, sect. 3.5.3 of Timmes et al. (1995) for a review on the situation in the early 1990's.) Actually, a nearly solar ratio was obtained even for extremely metal-poor stars ([Fe/H] down to ~ -4) by the extensive study of McWilliam et al. (1995b) using the resonance D lines (Na I 5890/5896). It should be pointed out that most of these previous studies were done based on the assumption of LTE.

In the late 1990's, however, new studies have appeared that cast doubt on this classical picture. Baumüller et al. (1998) investigated the non-LTE formation of various Na I lines and found considerable (negative) non-LTE corrections up to -0.5 dex for the D lines, which produced a systematic *decrease* of the [Na/Fe] ratio toward the metal-poor regime ([Na/Fe] ~ -0.5 at [Fe/H] ~ -3). Similarly, the (LTE) analysis of Stephens (1999) for halo dwarf stars based on high-quality spectra of Na I 5683/5688 subordinate lines suggested that [Na/Fe] progressively decreases to ~ -0.5 as [Fe/H] decreases from ~ -1 to ~ -2.

Accordingly, it appears that a proper account of the non-LTE effect is mandatory for studying the stellar sodium abundances, at least for the resonance Na I 5890/5896 D lines that are visible even in extremely metal-poor stars. Then, what about other subordinate lines, such as Na I 6154/6161 lines (widely used for relatively metal-rich population I disk stars), 5683/5688 lines (often used for typical halo stars with [Fe/H] of -1 to -2), 8183/8195 lines (not so popular due to their unfavorable wavelength location but potentially useful abundance indicators because of their clear visibility even down to [Na/H] ~ -3)? Do they also suffer an appreciable non-LTE effect? Any definite conclusion on the Galactic [Na/Fe] vs. [Fe/H] behavior should await until this problem is clarified, because different lines are used in different cases depending on the stellar metallicity.

We are aware that several elaborate and important studies have recently been done concerning the non-LTE effect on Na abundance determinations for solar-type stars (e.g., Baumüller et al. 1998; Gratton et al. 1999; Korotin & Mishenina 1999; Mashonkina et al. 2000). We would say, however, that their results are not presented in sufficient detail for the purpose of practical applications; i.e., they tend to be confined to only specific lines of interest or only to representative atmospheric parameters, and it is not always easy for the reader to assess how all those Na I lines of importance are affected by the non-LTE effect in stars comprising a diversity of atmospheric parameters.

In view of this circumstance, we decided (1) to carry out non-LTE calculations on the neutral sodium for a wide range of atmospheric parameters with an intention of applying to those 4 line pairs mentioned above, (2) to construct useful grids of non-LTE corrections, and (3) to perform extensive abundance analysis towards establishing the Na abundances of disk/halo stars with a variety of metallicities based on our own new observations/measurements along with the published equivalent widths taken from various sources in the literature.

The following sections of this paper are organized as follows. Our statistical-equilibrium calculations on neutral sodium and the resulting non-LTE corrections are explained in Sect. 2, where we also discuss the uncertain factors or adopted approximations involved in the abundance determination based on certain theoretical test calculations. Our observational data obtained at two observatories are explained in Sect. 3; this is followed by Sect. 4 where we describe the procedures of the abundance analysis using these data along with a reanalysis of the extensive literature data. We discuss in Sect. 5 the results obtained in Sect. 4, especially as regards the [Na/Fe] vs. [Fe/H] relation and its implications with reference to the representative theoretical calculations of Galactic chemical evolution. Finally, the conclusion of this paper is presented in Sect. 6.

2 NON-LTE CALCULATIONS

2.1 Computational Procedures

The procedures of our statistical-equilibrium calculations of neutral sodium, based on a Na I atomic model comprising 92 terms and 178 radiative transitions, are essentially the same as those described in Takeda & Takada-Hidai (1994) and Takeda (1995), which should be consulted for details. One difference is the choice of the background model atmospheres; i.e., instead of Kurucz's (1979) ATLAS6 models adopted in those previous works, the photoionizing radiation field was computed based on Kurucz's (1993a) ATLAS9 model atmospheres while incorporating the line opacity with the help of Kurucz's (1993b) opacity distribution functions. It should also be mentioned that a reduction factor of 0.1 (logarithmic correction of $h = -1$ according to the definition of Takeda 1995) was applied to the H I collision rates computed with the classical approximate formula (Steenbock & Holweger 1984; Takeda 1991) according to the empirical determination of Takeda (1995), though test calculations by varying this correction factor from 1 to 10^{-3} were also performed (cf. Sect. 2.3 below).

Since we planned to make our calculations applicable to stars from near-solar metallicity (population I) down to very low metallicity (extreme population II) at late-F through early-K spectral types in various evolutionary stages (i.e., dwarfs, subgiants, giants, and supergiants), we carried out non-LTE calculations on an extensive grid of 125 ($5 \times 5 \times 5$) model atmospheres resulting from combinations of five $T_{\rm eff}$ values (4500, 5000, 5500, 6000, 6500 K), five $\log g$ values (1.0, 2.0, 3.0, 4.0, 5.0), and five metallicities (represented by [Fe/H]) (0.0, −1.0, −2.0, −3.0, −4.0). As for the stellar model atmospheres, we adopted Kurucz's (1993a) ATLAS9 models corresponding to a microturbulent velocity (ξ) of 2 km s^{-1}.

Regarding the sodium abundance used as an input value in the non-LTE calculations, we assumed $\log \epsilon_{\rm Na}^{\rm input} = 6.33 +$ [Fe/H], where the solar sodium abundance of 6.33 was adopted from Anders & Grevesse (1989) (which is used also in the ATLAS9 models). That is, a metallicity-scaled sodium abundance was assigned to metal-poor models. The microturbulent velocity (appearing in the line-opacity calculations along with the abundance) was assumed to be 2 km s^{-1}, to make it consistent with the model atmosphere.

2.2 Characteristics of the Non-LTE Effect

In Fig. 1 are shown the $S_{\rm L}(\tau)/B(\tau)$, the ratio of the line source function to the Planck function, which is nearly equal to $\simeq b_{\rm u}/b_{\rm l}$, the ratio of the non-LTE departure coefficients between the upper and lower levels, and $l_0^{\rm NLTE}(\tau)/l_0^{\rm LTE}(\tau)$, the NLTE-to-LTE line-center opacity

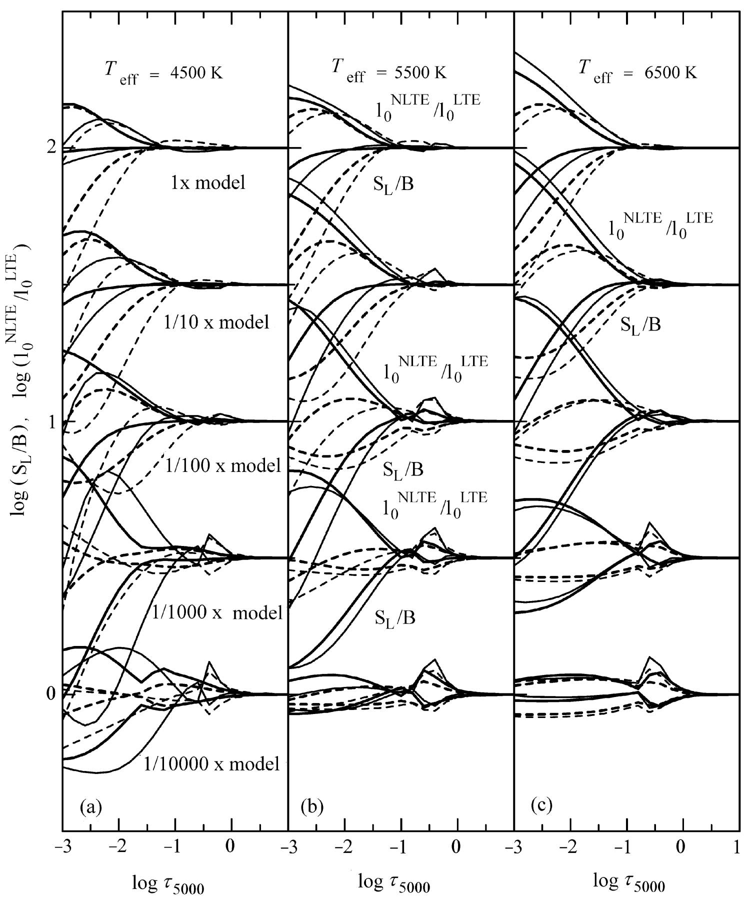

Fig. 1 Ratio of the line source function ($S_{\rm L}$) to the local Planck function (B) and the NLTE-to-LTE line-center opacity ratio as functions of the standard continuum optical depth at 5000 Å computed for models of $T_{\rm eff}$ = 4500 K, 5500 K, and 6500 K. Note that $S_{\rm L}/B$ and $l_0^{\rm NLTE}/l_0^{\rm LTE}$ are drawn in the same line-type, but the two are easily distinguished since the former (being diluted) is generally lower than the latter (overpopulated). The solid lines show the results for the 3 ^{2}S–3p ^{2}P$^{\rm o}$ transition of multiplet 1 (corresponding to the Na I 5890/5896 resonance lines), while those for the 3p ^{2}P$^{\rm o}$–3d ^{2}D transition of multiplet 4 (corresponding to the Na I 8183/8195 lines) are drawn in dashed lines. In each case, the results for two different gravity atmospheres are given: The thick lines for $\log g = 4$ and the thin lines for $\log g = 2$. The curves are vertically offset by 0.5 dex for clarity.

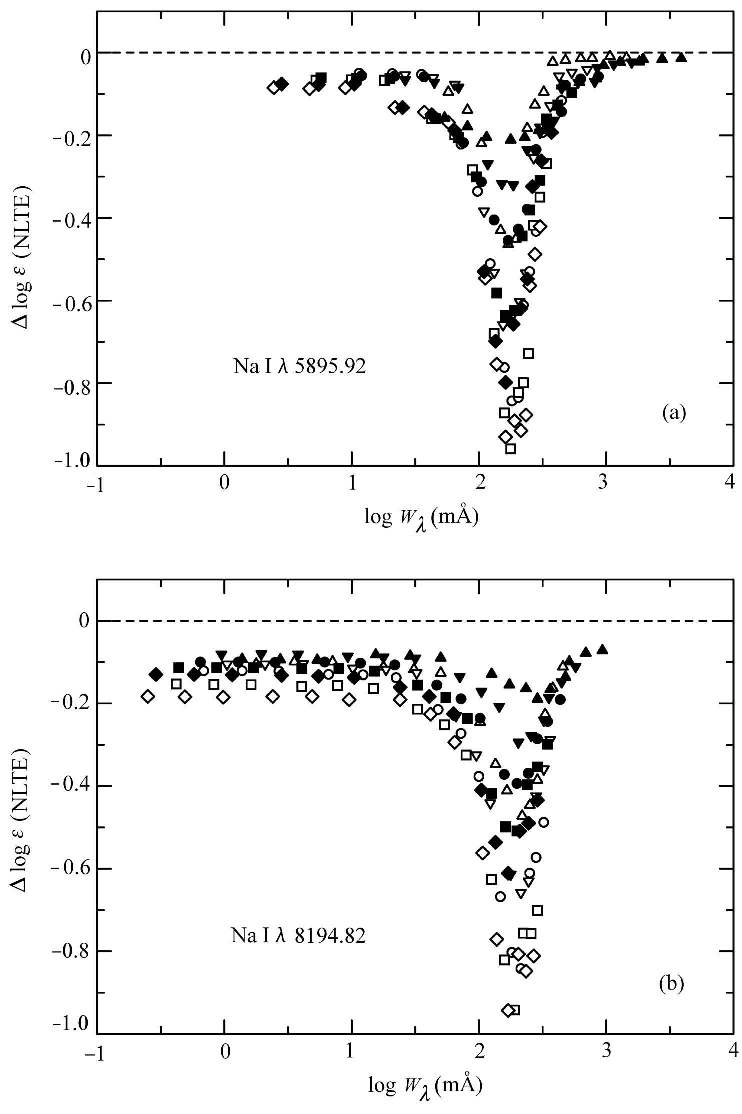

Fig. 2 Theoretical non-LTE corrections as functions of the NLTE equivalent width for representative models, based on the electronic Tables E1 (see Sect. 2.3 for details). Different symbols distinguish the different effective temperatures (triangles, deltas, circles, squares, and diamonds correspond to $T_{\rm eff}$ = 4500, 5000, 5500, 6000, and 6500 K, respectively) and open and closed symbols distinguish $\log g$ = 2 and 4. Shown are the results derived for five different model-metallicities ([Fe/H] = 0, −1, −2, −3, and −4), while using the metallicity-scaled sodium abundance along with variations of ±0.3 dex. (a) Na I 5895.92. (b) Na I 8194.82.

ratio, which is nearly equal to $\simeq b_l$ for each of the multiplet 1 (5890/5896) and multiplet 4 (8183/8195) transitions (non-LTE effects are especially important for these two doublets; cf. Sect. 5.1) for a representative set of model atmospheres. We can read the following characteristics from this figure, which are mostly the same as those obtained for the case of K I 7699 (Takeda et al. 2002):

— In almost all cases, the inequalities $S_\mathrm{L}/B < 1$ (dilution of line source function) and $l_0^\mathrm{NLTE}/l_0^\mathrm{LTE} > 1$ (enhanced line-opacity) hold in the important line-forming region for both cases of multiplets 1 and 4, which means that the non-LTE effect almost always acts in the direction of strengthening the 5890/5896 and 8183/8195 lines.[1] Actually, the more important is the former S_L-dilution effect which appreciably deepens/darkens the core of saturated lines to an extent that would never be reached under the assumption of LTE (where the residual intensity cannot be lower than $B(\tau \sim 0)/B(\tau \sim 1)$); hence, this raises the flat part of the curve of growth, and if this increase in the saturated-line strength is to be accounted for within the framework of LTE, a large abundance variation would have to be invoked. As a result, the extent of the non-LTE effect significantly depends on the line-strength in the sense that it becomes most conspicuous for the lines in the flat part. (See, e.g., Stürenburg & Holweger 1990, especially fig. 15 of sect. 4.3 therein.) This situation is demonstrated in Fig. 2, where the non-LTE corrections (see Sect. 2.3 below) for the 5896 and 8195 lines are shown as functions of the equivalent width for representative model atmospheres.

— There is a tendency that the non-LTE effect is enhanced with a lowering of the gravity, as naturally expected.

— The departure from LTE appears to be larger for higher T_eff in the high-metallicity (1×) case, while this trend becomes ambiguous, or even reversed, in the low-metallicity case.

— As the metallicity decreases, the extent of the non-LTE departure tends to decrease, but the departure appears to penetrate deeper into the atmosphere, which makes the situation rather complex.

— For a very strong damping-dominated case (i.e., lowest T_eff and highest metallicity), the departure from LTE shifts toward the upper atmosphere and the non-LTE effect becomes comparatively insignificant.

2.3 Grid of Non-LTE Corrections

Based on the results of these calculations, we computed extensive grids of the theoretical equivalent-widths and the corresponding non-LTE corrections for the considered eight lines (Na I 5683, 5688, 5890, 5896, 6154, 6161, 8183, and 8195) for each of the model atmospheres as follows.

For an assigned sodium abundance (A^a) and microturbulence (ξ^a), we first calculated the non-LTE equivalent width (W^NLTE) of the line by using the computed non-LTE departure coefficients (b) for each model atmosphere. Next, the LTE (A^L) and NLTE (A^N) abundances were computed from this W^NLTE while regarding it as if it were an observed equivalent width. We can then obtain the non-LTE abundance correction, Δ, which is defined in terms of these two abundances as $\Delta \equiv A^\mathrm{N} - A^\mathrm{L}$.

Strictly speaking, the departure coefficients ($b(\tau)$) for a model atmosphere are applicable only to the case of the input sodium abundance ($\log \epsilon_\mathrm{Na}^\mathrm{input}$) and microturbulence (2 km s^{-1}) adopted in the non-LTE calculations (cf. Sect. 2.1). Nevertheless, considering the fact that

[1] An exception is the case of lowest $T_\mathrm{eff}/\log g$ (e.g., T_eff=4500 K, $\log g = 1.0$, [Fe/H] = 0.0), where the line can be marginally weakened (i.e., positive abundance correction) by the enhanced S_L over B in the line-forming region (cf. the footnote in Sect. 5.3).

the departure coefficients (i.e., *ratios* of NLTE to LTE number populations) are (unlike the population itself) not very sensitive to small changes in the atmospheric parameters, we also used the b values so computed to evaluate Δ for slightly different $A^{\rm a}$ and $\xi^{\rm a}$ from those fiducial values assumed in the statistical equilibrium calculations. Thus, we evaluated Δ for three $A^{\rm a}$ values ($\log \epsilon_{\rm Na}^{\rm input}$ and ± 0.3 dex variations) as well as three ξ values (2 km s^{-1} and ± 1 km s^{-1} variations) for a model atmosphere using the same departure coefficients.

We used the WIDTH9 program (Kurucz 1993a), which had been modified to incorporate the non-LTE departure in the line source function as well as in the line opacity, for calculating the equivalent width for a given abundance, or inversely evaluating the abundance for an assigned equivalent width. The adopted line data (gf values, radiation damping constants, etc.) are given in Table 1.

Table 1 Adopted Atomic Data of the Na I Lines

Mult.	Line	λ	χ	$\log gf$	$\Gamma_{\rm R}$
1	λ5890	5889.95	0.00	+0.12	0.62
1	λ5896	5895.92	0.00	−0.18	0.62
4	λ8183	8183.26	2.10	+0.22	1.13
4	λ8195	8194.82	2.10	+0.52	1.13
5	λ6154	6154.23	2.10	−1.56	0.75
5	λ6161	6160.75	2.10	−1.26	0.75
6	λ5683	5682.63	2.10	−0.67	0.81
6	λ5688	5688.21	2.10	−0.37	0.81

Notes. The columns give, in order, the multiplet number, the line abbreviation used in this paper, the line wavelength (in Å), the lower excitation potential (in eV), the logarithm of the gf value, and the radiation damping constant in units of 10^8 s^{-1}. The data presented here are based on table 1 of Takeda & Takada-Hidai (1994), who consulted the compilation of Wiese et al. (1969). Each line was treated as if it is a single line, neglecting any hyperfine structure (cf. Sect. 2.3). See also Sect. 2.3 for the treatment of the quadratic Stark effect damping and of the van der Waals effect damping.

One of the controversial factors in abundance determinations for late-type stars is the choice of the van der Waals effect damping constant. Regarding this parameter, we assumed the classical Unsöld's (1955) formula unchanged, which means the adoption of $\Delta \log C_6 = 0.0$ (C_6 is connected to the damping width as $\log \Gamma_6 = \log \Gamma_6^{\rm classical} + 0.4 \Delta \log C_6$). While this choice is based on our previous empirical investigations (cf. appendix A of Takeda & Takada-Hidai 1994; sect. 4.2 of Takeda 1995), we actually confirmed that this choice is reasonable from the analysis of solar Na I lines (cf. Sect. 4.2). Anyhow, the precise value of this correction is not very essential unless very strong lines are used, as can be seen from Fig. 3 where the abundance changes expected by using $\Delta \log C_6 = 0.5$ are graphically displayed: the maximum change is $\sim 0.4 |\Delta \log C_6|$ which occurs in the case of very strong damping-dominated lines in low-temperature condition where Γ_6 dominates in Γ ($\equiv \Gamma_{\rm R} + \Gamma_4 + \Gamma_6$). Regarding the quadratic Stark effect damping (Γ_4, which is comparatively insignificant in late-type stars), we followed the Peytremann formula (Kurucz 1979, p.8).

Note also that we neglected the hyperfine structure (see, e.g., table 4 of McWilliam et al. 1995b for the 5890/5896 lines, and table 1 of Takeda & Takada-Hidai 1994 for the 8195 line) and treated each line as being purely single, because of a technical reason.[2] However, this does not cause any serious effect (several hundredths dex in most cases of practical importance) as illustrated in Fig. 4.

As an illustration of the non-LTE corrections, Table 2 gives the $\xi = 1$ km s^{-1} results for the Na I 5896 and 8195 lines computed for representative parameters [chosen to be nearly compatible with Baumüller et al.'s (1998) calculations] for the values $h = 0, -2, -3$ in addition

[2] We decided to invoke the original WIDTH9 algorithm (applicable to a symmetric single line) for the equivalent-width calculation instead of using the spectral-synthesis technique (which requires a sufficiently fine division of a line profile unsuited/unnecessary for very strong lines), since we wanted to treat cases of considerably different line strengths in the same consistent way (i.e., for constructing the tables of non-LTE corrections for different lines over wide parameter ranges).

to the fiducial value $h = -1$ (h is the logarithmic H I collision correction). Comparing this Table 2 with Baumüller et al.'s (1998) table 2 (where they adopted $10^h = 0.05$ or $h = -1.3$), we can see that our $|\Delta|$ values are quantitatively somewhat larger than theirs, though the qualitative tendency is in good agreement. The complete results (for all combinations of $T_{\rm eff}$, $\log g$, ξ values for each of the 8 lines, though only for the fiducial case of $h = -1$), are available only in electronic form. These tables (named "Tables E1") are at the ChJAA website: www.chjaa.org.

Table 2 Dependence of the non-LTE Effect on the Choice of the Correction Factor for the H I Collision

$T_{\rm eff}$	$\log g$	[Fe/H]	ξ	$A^{\rm a}$	λ	W_0	W_{-1}	W_{-2}	W_{-3}	Δ_0	Δ_{-1}	Δ_{-2}	Δ_{-3}
5500	4.0	0.0	1.0	6.33	5895.92	602.6	616.6	616.6	631.0	−0.04	−0.06	−0.06	−0.06
5500	4.0	−1.0	1.0	5.33	5895.92	309.0	316.2	331.1	331.1	−0.10	−0.15	−0.17	−0.18
5500	4.0	−2.0	1.0	4.33	5895.92	158.5	173.8	177.8	177.8	−0.26	−0.37	−0.40	−0.41
5500	4.0	−3.0	1.0	3.33	5895.92	85.1	89.1	91.2	89.1	−0.24	−0.33	−0.35	−0.33
5500	4.0	−4.0	1.0	2.33	5895.92	20.0	20.9	21.4	20.9	−0.03	−0.06	−0.06	−0.05
6500	4.0	0.0	1.0	6.33	5895.92	263.0	269.1	275.4	275.4	−0.18	−0.21	−0.21	−0.22
6500	4.0	−1.0	1.0	5.33	5895.92	169.8	177.8	182.0	182.0	−0.47	−0.55	−0.56	−0.56
6500	4.0	−2.0	1.0	4.33	5895.92	109.7	114.8	114.8	114.8	−0.61	−0.71	−0.72	−0.72
6500	4.0	−3.0	1.0	3.33	5895.92	38.0	39.8	39.8	38.9	−0.13	−0.16	−0.16	−0.16
6500	4.0	−4.0	1.0	2.33	5895.92	5.1	5.4	5.4	5.4	−0.06	−0.08	−0.08	−0.08
5500	4.0	0.0	1.0	6.33	8194.82	295.1	309.0	316.2	316.2	−0.15	−0.20	−0.21	−0.22
5500	4.0	−1.0	1.0	5.33	8194.82	154.9	173.8	182.0	186.2	−0.20	−0.35	−0.42	−0.44
5500	4.0	−2.0	1.0	4.33	8194.82	57.5	66.1	69.2	70.8	−0.08	−0.20	−0.25	−0.26
5500	4.0	−3.0	1.0	3.33	8194.82	10.0	11.8	12.3	12.3	−0.03	−0.10	−0.13	−0.13
5500	4.0	−4.0	1.0	2.33	8194.82	1.1	1.3	1.4	1.4	−0.03	−0.10	−0.12	−0.12
6500	4.0	0.0	1.0	6.33	8194.82	199.5	213.8	213.8	218.8	−0.34	−0.43	−0.47	−0.47
6500	4.0	−1.0	1.0	5.33	8194.82	107.2	117.5	123.0	123.0	−0.38	−0.55	−0.60	−0.61
6500	4.0	−2.0	1.0	4.33	8194.82	34.7	38.0	38.9	38.9	−0.12	−0.19	−0.21	−0.21
6500	4.0	−3.0	1.0	3.33	8194.82	4.9	5.5	5.6	5.6	−0.09	−0.13	−0.14	−0.14
6500	4.0	−4.0	1.0	2.33	8194.82	0.5	0.6	0.6	0.6	−0.09	−0.13	−0.14	−0.14

Notes. Cols. 1–6 are self-explanatory (the units of $T_{\rm eff}$, g, and ξ are K, cm s^{-2}, and km s^{-1}, respectively). The suffixes (0, −1, −2, −3, and −4) appended to W (the non-LTE equivalent width in mÅ calculated for the atmospheric parameters and the assigned sodium abundance given in Cols. 1–5) and Δ (the non-LTE abundance correction) denote the values of h (the logarithm of the H I collision correction factor applied to the classical formula).

3 OBSERVATIONAL DATA

Our observational data come from two observatories, Beijing Astronomical Observatory (BAO; 2.16 m reflector + coudé echelle spectrograph at Xinglong station) in P. R. China and Okayama Astrophysical Observatory (OAO; 1.9 m reflector + coudé HIgh-Dispersion Echelle Spectrograph named "HIDES") in Japan.

3.1 BAO Data

The BAO spectra ($R \sim 40000$ and S/N $\sim$ 200–400) used here are those originally collected for the purpose of Chen et al.'s (2000) comprehensive analyses on Galactic disk stars. See Sect. 2.2 therein for detailed information on the observations and the data quality. Chen et al. (2000) determined the abundance of sodium based on the comparatively weak Na I 6154/6161 lines, though the used equivalent-widths data were not published. For the present study, additional measurements for five lines (Na I 5683, 5688, 5890, 5896, and 8195; the 8183 line was discarded because of contamination of telluric lines) were newly carried out by one of us (Y.-Q. Chen; cf. sect. 2.3 of Chen et al. 2000 for the measurement method) on the spectra of 22 F–G stars (+ Moon), which are our BAO program stars also adopted in our previous potassium analysis (Takeda et al. 2002)[3] . Although many lines (except the 6154/6161 lines) are so strong in these disk stars that they are not suitable for sodium abundance determination, we tried to derive their abundances in order to see whether similar behavior of [Na/Fe] may be reproduced among the different line groups (cf. Sect. 5.2). Yet, it should be kept in mind that greater or lesser errors are involved in measuring the equivalent widths of very strong damping-dominated lines such as the 5890/5896 D lines. Nevertheless, comparing the solar (Moon) equivalent width measured by us with those taken from the literature (cf. Table 3), we can see that our measurements are reasonable (i.e., crucial systematic discrepancies are not observed). The finally obtained BAO equivalent-widths are given in Tables 4 and 5.

Table 3 Comparison of the Solar Equivalent Widths (in mÅ) of Na I Lines taken from Various Sources

Ref.	λ5683	λ5688	λ5890	λ5896	λ6154	λ6161	λ8183	λ8195	Data source
(1)	100.4	131.1	837.2	545.0	38.6	59.5	···	306.1	BAO Moon[a]
(2)	105.3	128.6	···	···	···	···	···	···	B76 solar flux
(3)	106.9	127.9	···	···	···	···	···	···	B76 solar flux
(4)	106.9	127.9	···	···	36.8	58.6	···	···	B76 solar flux
(5)	···	129.0	1125.5	736.5	···	···	257.3	326.6	solar flux & disk center[b]
(6)	···	···	···	···	35.0	53.7	···	···	solar disk center[c]
(7)	90.0	119.1	···	···	40.5	58.2	···	···	K84 solar flux
(8)	121	144	830	640	41	63	254	328	K84 solar flux
(9)	···	···	756	597	···	···	244	315	K84 solar flux[d]
(10)	103.0	128.0	···	···	36.0	···	···	···	From (12)?
(11)	···	···	···	···	38.6	59.5	···	···	K84 solar flux
(12)	103	128	765	570	36	53	239	322	solar disk center[e]

References: (1) This study; (2) Peterson & Carney (1979); (3) Peterson (1980); (4) Peterson (1981); (5) Gratton & Sneden (1987b); (6) Tomkin et al. (1985); (7) Prochaska et al. (2000); (8) Mashonkina et al. (2000); (9) Takeda (1995); (10) Carretta et al. (2000); (11) Sadakane et al. (2002); (12) Holweger (1971).
Notes on the data sources:
B76 and K84 means the solar flux spectrum atlas published by Beckers et al. (1976) and Kurucz et al. (1984), respectively.
[a] Moon spectrum observed at Beijing Astronomical Observatory.
[b] Based on two different atlases (see Gratton & Sneden 1987a).
[c] Taken from the values published by Lambert & Luck (1978), which are based on two different atlases.
[d] Inversely computed from the profile fitting solutions.
[e] Based on three different atlases.

3.2 OAO Data

The OAO data are based on the near-IR spectra of 17 mostly metal-poor disk/halo stars (dwarfs and giants being mixed), which have been collected by using HIDES during our observing runs in 2001–2002.[4] The slit width of 250 μm (0.95″) was set to yield a spectral resolution of $R \sim 50000$. By using the single 4K×2K CCD (pixel size of 13.5 μm × 13.5 μm), a wavelength

[3] One of our present 22 BAO stars, HD 167588, was not included in Takeda et al.'s (2002) analysis, because there was a problem in the data quality of the K I 7699 line.

[4] Actually, the primary motivation of these observations was to study the abundance of sulfur based on the near-IR S I lines. However, we could use those spectra for the present purpose, since they cover the wavelength region of the Na I 8183/8195 lines.

span of $\sim$ 1100 Å could be covered. Most of our observations were made in the wavelength region of $\sim$ 7700–8800 Å.

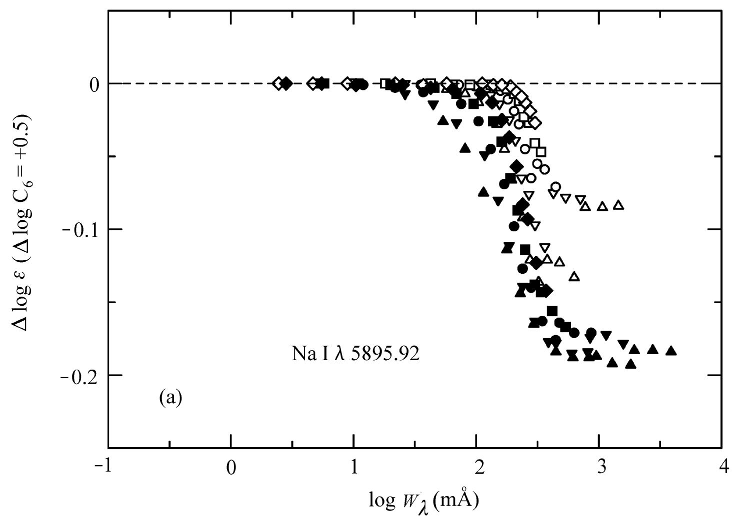

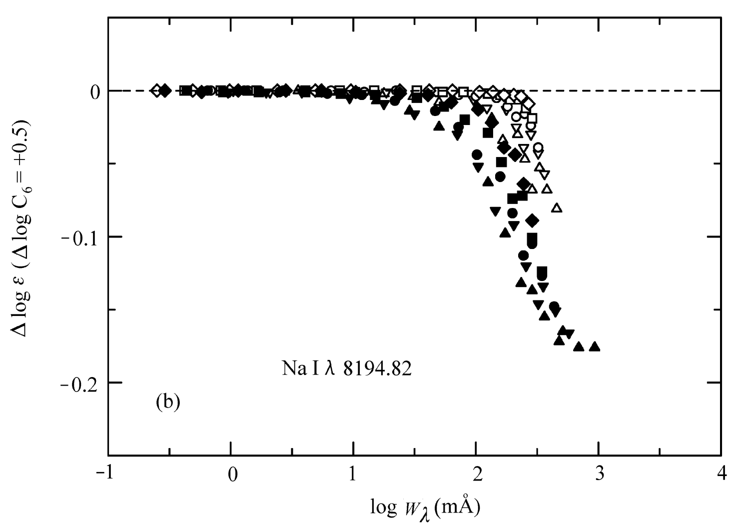

Fig. 3 Differences of the resulting non-LTE abundances, when $\Delta \log C_6 = +0.5$ (logarithmic correction applied to classical value of the van der Waals effect damping parameter) was used instead of the fiducial value of $\Delta \log C_6 = 0.0$, as functions of the non-LTE equivalent widths for the representative cases shown in Table 2. See the caption of Fig. 2 for the meanings of the symbols. (a) Na I 5895.92. (b) Na I 8194.82.

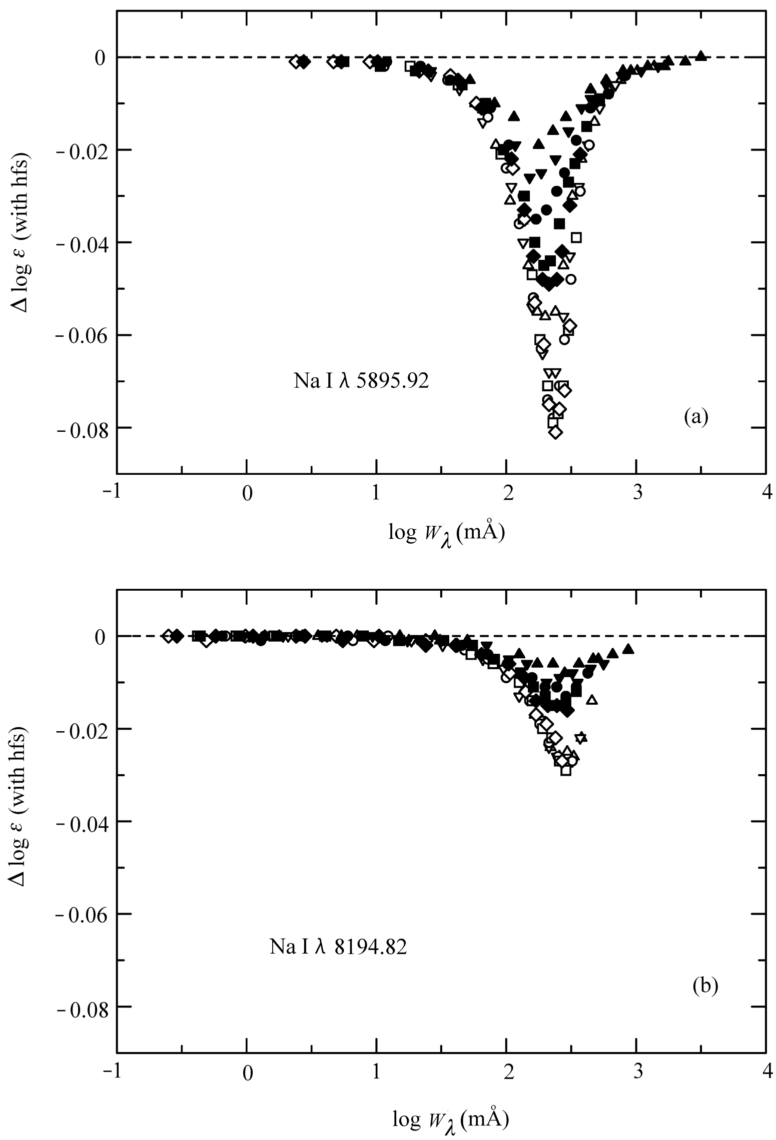

Fig. 4 Differences of the resulting non-LTE abundances, when hyperfine structure was approximately included instead of the purely single-line treatment (as basically adopted in this study; cf. Table 1), as functions of the non-LTE equivalent widths for the representative cases. See the caption of Fig. 2 for the meaning of the symbols. (a) Na I λ5896 [using the two-component approximation of $gf(5895.93) = 0.269$ and $gf(5895.95) = 0.376$; cf. McWilliam et al. 1995b)]. (b) Na I λ8195 [using the two-component approximation of $gf(8194.79) = 0.332$ and $gf(8194.82) = 2.999$; cf. Wiese et al. 1969].

Table 4 Analysis of Na I 8183/8195 Lines based on the BAO and OAO Data

Star	Sp. type	$T_{\rm eff}$	$\log g$	[Fe/H]	ξ	W_{8183}	$A^{\rm N}_{8183}$	Δ_{8183}	W_{8195}	$A^{\rm N}_{8195}$	Δ_{8195}	Ref.
[BAO sample]												
Sun	G2 V	5780	4.44	0.00	1.0	···	···	···	306.1	6.32	−0.19	(1)
HD 010307	G1.5 V	5776	4.13	−0.05	1.8	···	···	···	265.5	6.08	−0.31	(1)
HD 019373	G0 V	5867	4.01	+0.03	1.8	···	···	···	274.8	6.23	−0.32	(1)
HD 022484	F9 IV-V	5915	4.03	−0.13	2.0	···	···	···	242.5	5.97	−0.39	(1)
HD 034411	G1.5 IV-V	5773	4.02	+0.01	1.7	···	···	···	275.8	6.20	−0.30	(1)
HD 039587	G0 V	5805	4.29	−0.18	2.2	···	···	···	273.9	5.99	−0.32	(1)
HD 041640	F5	6004	4.37	−0.62	2.0	···	···	···	205.6	5.65	−0.39	(1)
HD 049732	F8	6260	4.15	−0.70	1.9	···	···	···	178.3	5.63	−0.50	(1)
HD 055575	G0 V	5802	4.36	−0.36	1.6	···	···	···	···	···	···	(1)
HD 060319	F8	5867	4.24	−0.85	1.6	···	···	···	171.4	5.41	−0.39	(1)
HD 062301	F8 V	5837	4.23	−0.67	1.7	···	···	···	190.1	5.53	−0.38	(1)
HD 068146	F7 V	6227	4.16	−0.09	2.1	···	···	···	229.4	6.01	−0.42	(1)
HD 069897	F6 V	6243	4.28	−0.28	2.0	···	···	···	197.5	5.77	−0.42	(1)
HD 076349	G0	6004	4.21	−0.49	2.1	···	···	···	210.9	5.69	−0.43	(1)
HD 101676	F6 V	6102	4.09	−0.47	2.0	···	···	···	214.8	5.82	−0.47	(1)
HD 106516	F5 V	6135	4.34	−0.71	1.5	···	···	···	168.6	5.55	−0.41	(1)
HD 109303	F8	5905	4.10	−0.61	1.7	···	···	···	186.5	5.56	−0.43	(1)
HD 118244	F5 V	6234	4.13	−0.55	2.3	···	···	···	197.7	5.68	−0.50	(1)
HD 142373	F8 Ve	5920	4.27	−0.39	1.5	···	···	···	···	···	···	(1)
HD 142860	F6 IV	6227	4.18	−0.22	2.2	···	···	···	211.5	5.84	−0.44	(1)
HD 167588	F8 V	5894	4.13	−0.33	1.7	···	···	···	···	···	···	(1)
HD 201891	F8 V-IV	5827	4.43	−1.04	1.6	···	···	···	152.6	5.21	−0.33	(1)
HD 208906	F8 V-IV	5929	4.39	−0.73	1.5	···	···	···	173.9	5.47	−0.36	(1)
[OAO sample]												
HD 6833	G9 III	4450	1.40	−0.90	1.6	161.3	4.92	−0.41	207.9	5.10	−0.46	(2)
HD 26297	G5/G6 Ivw	4500	1.20	−1.60	1.7	86.4	4.24	−0.21	115.6	4.24	−0.32	(2)
HD 73394	G5 IIIw	4500	1.10	−1.40	1.5	127.7	4.71	−0.37	157.0	4.73	−0.46	(3)
HD 76932	F7/F8 IV/V	5900	4.12	−0.80	1.3	125.1	5.40	−0.38	155.6	5.37	−0.42	(4)[a]
HD 88609	G5 IIIw	4570	0.75	−2.70	1.9	10.8	3.18	−0.10	20.1	3.19	−0.11	(4)
HD 106516	F5 V	6200	4.31	−0.70	1.1	134.8	5.66	−0.41	167.1	5.65	−0.42	(4)[a]
HD 108317	G0	5300	2.90	−2.24	1.0	26.5	3.95	−0.16	41.0	3.91	−0.18	(5)
HD 122563	F8 IV	4590	1.17	−2.74	2.3	15.7	3.35	−0.11	31.5	3.41	−0.12	(6)
HD 140283	sdF3	5690	3.69	−2.42	0.8	6.0	3.38	−0.12	9.6	3.29	−0.13	(7)[a]
HD 165908	F7 V	5900	4.09	−0.60	1.7	143.2	5.51	−0.39	179.9	5.51	−0.43	(4)
HD 167588	F8 V	5890	4.13	−0.33	1.7	170.9	5.76	−0.38	205.3	5.72	−0.39	(1)
HD 187111	G8wvar	4260	0.51	−1.85	1.8	94.5	4.18	−0.19	147.6	4.41	−0.34	(6)
HD 189322	G8 III	4464	2.00	−1.57	2.0	222.1	5.37	−0.43	260.0	5.38	−0.38	(8)[b]
HD 216143	G5	4525	1.00	−2.10	2.9	50.0	3.86	−0.12	70.7	3.78	−0.15	(2)
HD 221170	G2 IV	4425	1.00	−2.15	1.5	53.0	3.91	−0.14	79.4	3.93	−0.20	(5)
BD +37°1458	G0	5200	3.00	−2.00	1.3	19.8	3.73	−0.15	42.7	3.86	−0.18	(2)
Procyon	F5 IV-V	6510	3.96	−0.05	2.2	188.7	6.14	−0.51	220.3	6.08	−0.53	(9)

Notes. Cols. 1–6 are self-explanatory as in Table 2. W is the observed equivalent width (in mÅ), $A^{\rm N}$ is the logarithmic non-LTE abundance (in the usual normalization of H = 12), and Δ is the non-LTE correction ($\equiv A^{\rm N} - A^{\rm L}$). Col. 13 gives the keys to the references of the atmospheric parameters (cf. Sect. 4.1): (1) Chen et al. (2000); (2) Fulbright (2000); (3) Luck & Bond (1985);(4) Takada-Hidai et al. (2002); (5) Pilachowski et al. (1996); (6) Gratton & Sneden (1994); (7) Nissen et al. (2002); (8) Alonso et al. (1999); (9) Allende Prieto et al. (2002).
[a] Only the ξ value was taken from (2).
[b] The ξ value was assumed.

The data reduction was performed with the IRAF[5] `echelle` package, following the standard procedure for extracting one-dimensional spectra. We also removed the telluric lines using the `telluric` task of IRAF and the spectra of a rapid rotator. The S/N ratios of the resulting spectra, differing from star to star, are typically of the order of 200–300. The resulting OAO

[5] IRAF is distributed by the National Optical Astronomy Observatories, operated by the Association of Universities for Research in Astronomy, Inc., under cooperative agreement with the National Science Foundation.

equivalent widths of the Na I 8183/8195 lines based on these spectra, which were measured by either Gaussian fitting or direct integration using the `splot` task of IRAF, are presented in Table 4. Note that, although two stars (HD 106516 and HD 167588) are common to BAO and OAO samples, they were treated independently.

Table 5 Analysis of Na I 5683/5688, 5890/5896, and 6154/6160 Lines based on the BAO Data

Star	W_{5683}	A^{N}_{5683}	Δ_{5683}	W_{5688}	A^{N}_{5688}	Δ_{5688}	W_{5890}	A^{N}_{5890}	Δ_{5890}	W_{5896}	A^{N}_{5896}	Δ_{5896}	W_{6154}	A^{N}_{6154}	Δ_{6154}	W_{6161}	A^{N}_{6161}	Δ_{6161}
[BAO sample]																		
Sun	100.4	6.28	−0.11	131.1	6.33	−0.13	837.2	6.41	−0.05	545.0	6.27	−0.07	38.6	6.31	−0.04	59.5	6.32	−0.06
HD 010307	⋯	⋯	⋯	134.3	6.26	−0.16	779.2	6.43	−0.07	506.5	6.30	−0.09	39.4	6.29	−0.05	60.6	6.28	−0.07
HD 019373	⋯	⋯	⋯	139.6	6.39	−0.19	⋯	⋯	⋯	⋯	⋯	⋯	45.8	6.44	−0.05	65.3	6.40	−0.07
HD 022484	⋯	⋯	⋯	116.9	6.12	−0.17	458.5	6.02	−0.12	402.6	6.16	−0.13	32.1	6.23	−0.06	47.1	6.17	−0.07
HD 034411	⋯	⋯	⋯	133.6	6.30	−0.17	795.3	6.52	−0.07	505.6	6.37	−0.08	39.7	6.30	−0.05	65.6	6.36	−0.07
HD 039587	⋯	⋯	⋯	118.1	6.01	−0.13	625.6	6.11	−0.09	459.5	6.06	−0.12	24.0	6.01	−0.05	48.4	6.11	−0.06
HD 041640	⋯	⋯	⋯	77.2	5.69	−0.12	413.1	5.69	−0.16	316.3	5.64	−0.21	9.1	5.63	−0.07	21.8	5.75	−0.07
HD 049732	⋯	⋯	⋯	73.7	5.78	−0.15	343.8	5.80	−0.24	260.8	5.65	−0.34	7.7	5.65	−0.08	17.3	5.74	−0.09
HD 055575	⋯	⋯	⋯	93.2	5.82	−0.12	⋯	⋯	⋯	412.6	5.90	−0.11	21.6	5.96	−0.05	36.2	5.95	−0.06
HD 060319	⋯	⋯	⋯	59.7	5.45	−0.11	354.5	5.42	−0.18	270.9	5.36	−0.23	6.3	5.40	−0.07	17.8	5.60	−0.08
HD 062301	⋯	⋯	⋯	71.8	5.58	−0.12	407.8	5.60	−0.14	285.8	5.43	−0.21	10.2	5.61	−0.07	19.9	5.64	−0.07
HD 068146	⋯	⋯	⋯	115.9	6.24	−0.17	436.3	6.19	−0.15	352.0	6.20	−0.18	24.6	6.23	−0.06	43.3	6.25	−0.07
HD 069897	⋯	⋯	⋯	94.1	6.01	−0.14	374.0	5.92	−0.18	306.3	5.92	−0.23	14.5	5.96	−0.06	29.1	6.02	−0.07
HD 076349	⋯	⋯	⋯	87.1	5.79	−0.14	401.0	5.74	−0.17	318.0	5.71	−0.22	14.7	5.85	−0.07	29.8	5.92	−0.08
HD 101676	⋯	⋯	⋯	93.0	5.93	−0.16	⋯	⋯	⋯	294.5	5.76	−0.27	15.3	5.92	−0.07	31.2	5.99	−0.08
HD 106516	⋯	⋯	⋯	69.9	5.71	−0.13	313.5	5.52	−0.21	260.6	5.56	−0.26	9.0	5.68	−0.07	22.1	5.82	−0.08
HD 109303	⋯	⋯	⋯	78.6	5.70	−0.14	382.4	5.66	−0.17	279.4	5.53	−0.23	8.1	5.53	−0.07	32.2	5.93	−0.08
HD 118244	⋯	⋯	⋯	91.9	5.93	−0.16	353.7	5.78	−0.25	281.9	5.68	−0.34	9.7	5.75	−0.08	29.5	6.00	−0.09
HD 142373	68.1	5.89	−0.10	⋯	⋯	⋯	407.0	5.75	−0.12	401.1	6.03	−0.13	12.6	5.75	−0.06	26.5	5.84	−0.07
HD 142860	⋯	⋯	⋯	106.3	6.11	−0.16	449.6	6.18	−0.16	317.6	5.98	−0.24	17.6	6.05	−0.06	44.0	6.25	−0.08
HD 167588	75.1	5.96	−0.11	97.4	5.92	−0.15	423.4	5.84	−0.13	368.4	5.96	−0.14	19.1	5.95	−0.06	37.6	6.02	−0.07
HD 201891	⋯	⋯	⋯	43.3	5.20	−0.09	328.1	5.14	−0.19	209.3	4.82	−0.28	7.4	5.46	−0.07	9.6	5.28	−0.07
HD 208906	52.1	5.68	−0.09	⋯	⋯	⋯	⋯	⋯	⋯	⋯	⋯	⋯	9.2	5.61	−0.07	21.3	5.72	−0.07

See the notes to Table 4 for the meanings of the W, A^{N}, and Δ.

4 Abundance Analyses

4.1 Atmospheric Parameters

First we need to establish the four atmospheric parameters, $T_{\rm eff}$ (effective temperature), $\log g$ (surface gravity), [Fe/H] (metallicity; represented by the Fe abundance relative to the Sun), and ξ (microturbulent velocity dispersion), which are necessary for constructing the model atmosphere and deriving the abundance from an equivalent width. Regarding the 22 BAO stars, the parameter data determined by Chen et al. (2000) were used unchanged, while the reasonably well known solar parameters of (5780 K, 4.44, 0.0, 1.0 km s^{-1}) were applied to the analysis of the BAO Moon data. For the 17 OAO stars, the atmospheric parameters were taken from the published values found in various papers (cf. Col. 13 of Table 4); when two or more references were available for the same star, we selected an appropriate value according to our personal judgement. The finally adopted values are given in Table 4.

As for the model atmospheres, Kurucz's (1993a) grid of ATLAS9 models was used as in the case of the non-LTE calculations, from which the model for each star was obtained by a three-dimensional interpolation with respect to $T_{\rm eff}$, $\log g$, and [Fe/H]. Similarly, the depth-dependent departure coefficients (b) of Na I levels computed for the grid of models (cf. Sect. 2) were interpolated, when evaluating the $S_{\rm L}(\tau)/B(\tau)$ and $l_0^{\rm NLTE}(\tau)/l_0^{\rm LTE}(\tau)$ ratios for each of the stars.

4.2 Abundance Determination

The procedures for determining the sodium abundances from the equivalent widths of Na I lines are the same as already explained in Sect. 2.3 (i.e., modified WIDTH9 program, line data given in Table 1, $\Delta \log C_6 = 0$, neglecting the hyperfine structures).

The resulting non-LTE abundance ($A^{\rm N}$) and the non-LTE abundance correction ($\equiv A^{\rm N} - A^{\rm L}$) derived for each line and for each star are presented in Tables 4 (8183/8195 lines) and 5 (5683/5688, 5890/5896, and 6154/6161 lines). As can be seen from these two tables, the solar non-LTE abundances derived from the BAO Moon equivalent widths of Na I 8195 (6.32), 5683 (6.28), 5688 (6.33), 5890 (6.41), 6154 (6.31), and 6160 (6.32) are in remarkable agreement with each other; moreover, their average of 6.32(σ = 0.04) is essentially the same as the standard solar sodium abundance of 6.33 (Anders & Grevesse 1989). Accordingly, we confirmed the internal consistency of using $\Delta \log C_6 = 0.0$, as far as our present analysis using ATLAS9 model atmospheres is concerned. (Actually, empirical determination of this correction significantly depends on the choice of the atmospheric models, as demonstrated in sect. 4.2 of Takeda (1995).)

The abundance changes caused by uncertainties in the atmospheric parameters are quantitatively similar to the case of potassium described in sect. 5 of Takeda et al. (2002), since K and Na have quite similar atomic structures to each other (alkali atom with one valence electron; ionization potential of 4–5 eV) and most atoms are in the once-ionized stage. Hence, even for changes of $\Delta T_{\rm eff} \sim \pm 200$ K or $\Delta \log g \sim \pm 0.3$ dex (we expect that internal errors in the parameters of our program stars, especially for BAO sample stars, are smaller than these), the extents of the resulting abundance variations are $\lesssim$ 0.2 dex, as can be seen from Table 1 of Takeda et al. (2002). The effect of changing the microturbulence, which influences only the lines at the flat part of the curve of growth ($W_\lambda \sim$ 100–300 mÅ; cf. Fig. 4) can also be assessed by inspecting that table.

The [Na/Fe] ratios (Na-to-Fe logarithmic abundance ratio relative to the Sun) can be obtained based on the results in Tables 4 and 5 as $A^{\rm N}$(star) − 6.33 − [Fe/H], where we assumed Anders & Grevesse's (1989) value of 6.33 as the reference solar Na abundance. The resulting [Na/Fe] vs. [Fe/H] relations derived from each of the four multiplets, along with the corresponding non-LTE corrections, are displayed in Fig. 5.

Note that when two lines of the same multiplet are available, we averaged the abundances ([Na/Fe]) as well as the non-LTE corrections for both lines and such derived mean results for the multiplet are shown.

4.3 Reanalysis of Published Data

We also tried to reanalyze the published equivalent-width data (for the Na I 5683/5688, 5890/5896, 6154/6161, and 8183/8195 lines) of late-type stars in the Galactic disk as well as in the halo covering a wide range of metallicities, while taking account of the non-LTE effect. In our search for the observational data we need, the extensive references quoted by Timmes et al. (1995), Samland (1998), and Goswami & Prantzos (2000) were quite helpful. Although our literature survey is not complete, we consider that we have included most of the important works done after the 1980's.

These data were analyzed just in the same way as we did for our BAO/OAO data (cf. Sects. 4.1 and 4.2). The atmospheric parameters were taken from the same paper as that presenting the equivalent-width data as far as possible.[6] By inspecting those original papers, we found that the analyses carried out before 1990 tend to be based on rather coarsely determined

[6] The exceptional cases are as follows: Gratton & Sneden's (1987b) EW data were analyzed with the parameters taken from Gratton & Sneden (1987a). Peterson's (1989) EW data were analyzed with the parameters of Peterson et al. (1990). Zhao & Magain's (1990b) EW data were analyzed with ($T_{\rm eff}$, $\log g$, and ξ) values taken from Magain (1989) and [Fe/H] values taken from Zhao & Magain (1990a). McWilliam et al.'s (1995a) EW data were analyzed with the parameters taken from McWilliam et al. (1995b).

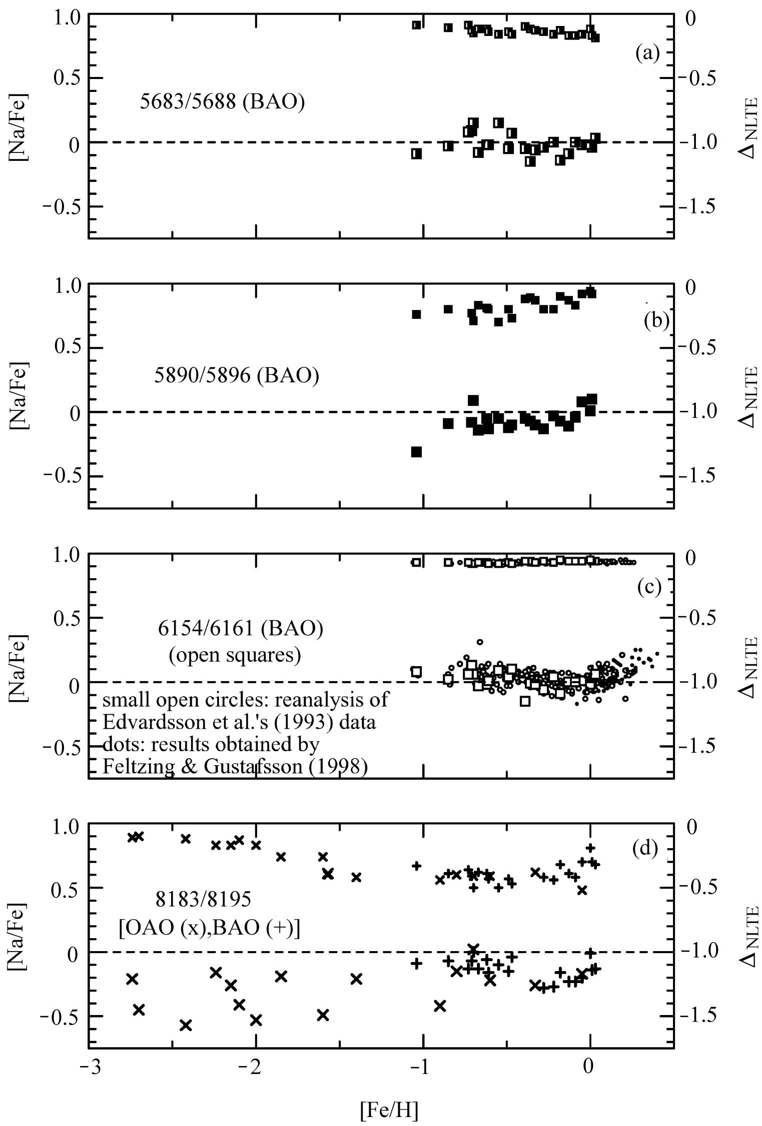

Fig. 5 [Na/Fe] values resulting from the non-LTE analysis of our BAO and OAO data (larger symbols; scale in the left-hand axis) and the corresponding non-LTE corrections (smaller symbols; scale in the right-hand axis), plotted as functions of [Fe/H]; these are based on the data presented in Tables 4 and 5. (a) $\lambda5683/\lambda5688$ lines of multiplet 6, plotted in half-filled squares (BAO). (b) $\lambda5890/\lambda5896$ lines of multiplet 1, plotted in filled squares (BAO). (c) $\lambda6154/\lambda6161$ lines of multiplet 5, plotted in open squares (BAO). The results of our reanalysis of Edvardsson et al.'s (1993) data (also depicted in Fig. 7a) and the results of Feltzing & Gustafsson (1998) (the LTE [Na/Fe] values obtained by themselves; their equivalent-width data are not published) are also shown with small open circles and dots, respectively, for a comparison. (d) $\lambda8183/\lambda8195$ lines of multiplet 4, plotted in Greek crosses (BAO) and St. Andrew's crosses (OAO), respectively.

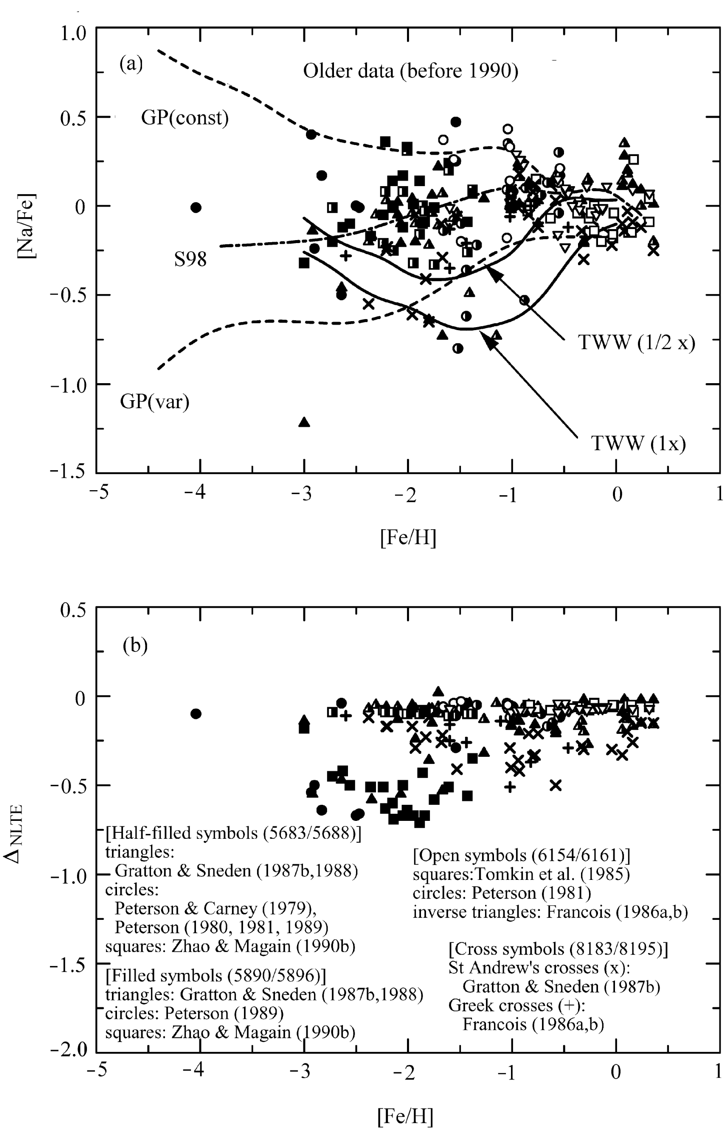

Fig. 6 (a) [Na/Fe] vs. [Fe/H] relation resulting from the non-LTE reanalysis of the rather old data published before 1990. See panel (b) for the data sources of equivalent widths and the corresponding symbols. Lines show the representative theoretical predictions: Dash-dotted line (S98)— taken from fig. 8 of Samland (1998), dashed line (TWW) — taken from fig. 17 of Timmes et al. (1995) corresponding to the two cases for the standard Woosley & Weaver's (1995) Fe yield from massive stars and the reduced one by a factor of 2 (which may be more reasonable according to their suggestion), dashed line — taken from fig. 7 of Goswami & Prantzos (2000), for the two cases of Na yield; time-independent constant yield (GP(const); only for a comparison purpose) and the realistic metallicity-dependent Na yield (GP(var)). (b) The corresponding NLTE corrections used for deriving the [Na/Fe] values shown in panel (a), plotted as functions of [Fe/H].

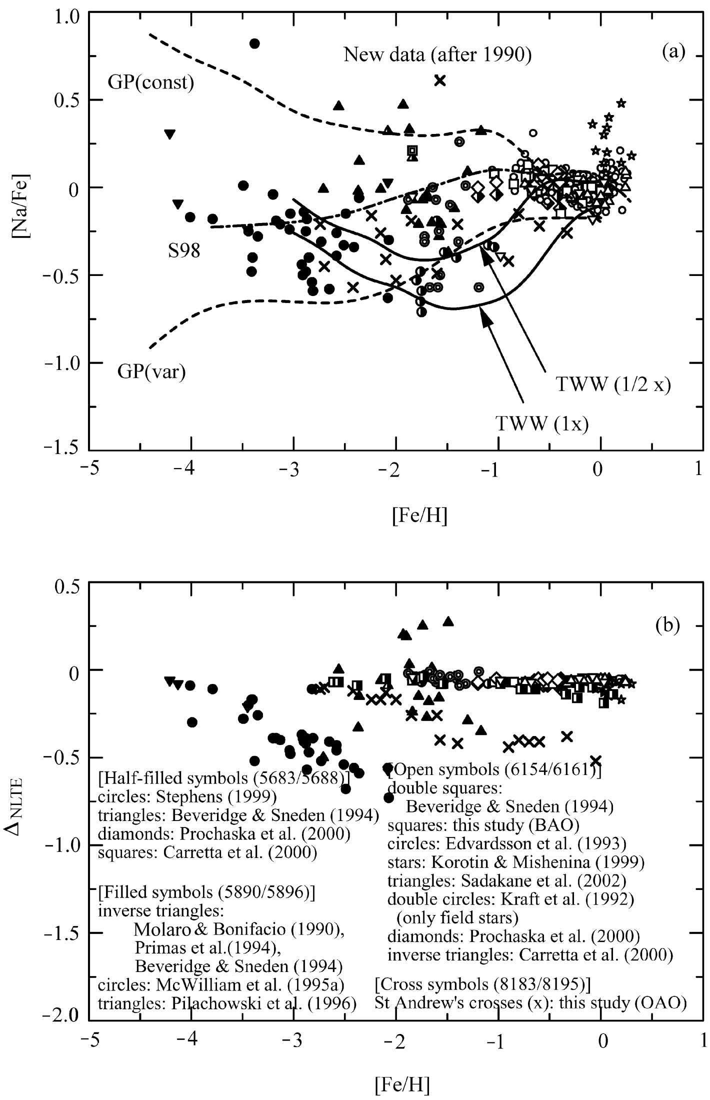

Fig. 7 (a) [Na/Fe] vs. [Fe/H] relation resulting from the non-LTE reanalysis based on the recently published new data after 1990. The data point for CS 22949-037 ([Na/Fe] = +1.94 at [Fe/H] = −3.99) derived from the reanalysis of McWilliam et al.'s (1995a) EW data is outside the plot range of this figure (cf. Fig. 8a for a more global view including this anomalous point). (b) The corresponding NLTE corrections used for deriving the [Na/Fe] values shown in panel (a), plotted as functions of [Fe/H]. Otherwise, the same as in Fig. 6; see the caption therein for more details. The results of the reanalysis of Pilachowski et al.'s (1996) 5890/5896 data for the low-gravity giants/supergiants (filled triangles) may suffer rather large uncertainties and should not be seriously taken (cf. the footnote in Sect. 5.3).

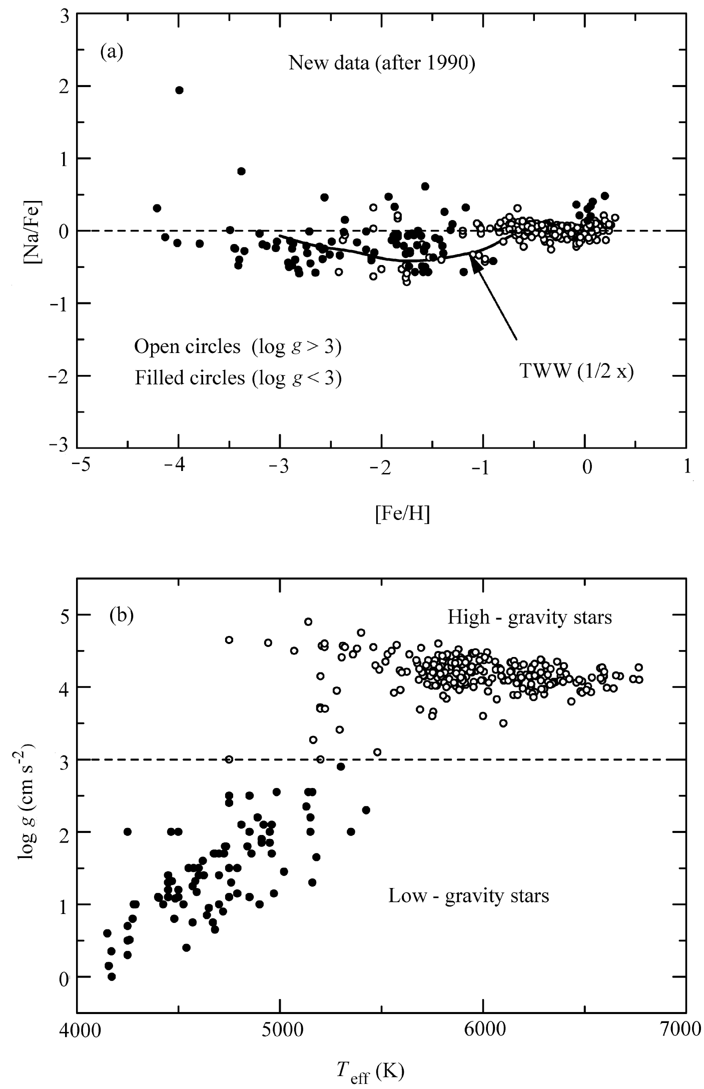

Fig. 8 (a) [Na/Fe] vs. [Fe/H] relation resulting from the non-LTE reanalysis of the newer published data after 1990. The plotted data are essentially the same as in Fig. 7a, but dwarfs and giants are distinguished by different symbols: open circles — high-gravity stars ($\log g \geq 3$), filled circles — low-gravity stars ($\log g < 3$). The theoretical prediction of Timmes et al. (1995) (the case of reduced Fe yield denoted by "TWW (1/2 $\times$)"; cf. the caption of Fig. 6a), which appears to match the observed trend most closely, is also drawn for comparison. (b) $T_{\rm eff}$ vs. $\log g$ relation for the sample stars relevant to the data plots in (a). The meanings of the symbols are the same as in (a).

parameters (e.g., using rounded $T_{\rm eff}$ or $\log g$ values; assuming the same ξ values for all program stars, etc.), compared to the more recent studies carried out in this past decade. Accordingly, we decided to present the results of the reanalysis on the data before and after 1990 separately. Figure 6 shows the resulting [Na/Fe] vs. [Fe/H] relations and the corresponding non-LTE corrections derived from the older data before 1990, while those obtained from the analyses of the recent data after 1990 are displayed in Fig. 7.[7]

The same results as those in Fig. 7a (the reanalysis results based on the newer data after 1990) are depicted in Fig. 8a, which plots the [Na/Fe] data on a more compressed vertical scale (for the purpose of clarifying the global tendency) and using different symbols to distinguish low- and high-gravity stars. In addition, Fig. 8b plots $T_{\rm eff}$ vs. $\log g$, relevant to these data; it can be seen from this figure that most of the high-gravity stars are comparatively higher $T_{\rm eff}$ stars of mid-F through late-G type, while low-gravity stars mainly consist of late-G through early-K giants of lower $T_{\rm eff}$ and show a positive correlation between $T_{\rm eff}$ and $\log g$ (reflecting the evolutionary sequence). Fig. 8a shows no meaningful systematic $\log g$-dependent difference in the [Na/Fe] values; however, the biased nature of the sample (i.e., very low-metallicity stars tend to be low-gravity giants, and vice versa) prevents us from making any definitive statement on this point.

The details of these analyses (the data of the used equivalent widths and the adopted parameter values, the resulting non-LTE abundances or [Na/Fe] values with the non-LTE corrections, given for each line/multiplet and for each star) are available only electronically as "Tables E2"(from the ftp site mentioned at the end of Sect. 2.3).

5 DISCUSSION

5.1 Non-LTE Effect

Figures 5, 6, and 7 clearly show how the non-LTE effect acts on different Na I lines in sodium abundance determinations for stars of various metallicities.

Roughly, a simple principle appears to hold: The non-LTE effect (negative corrections to the corresponding LTE abundances) tends to be most important for rather strong saturated lines (with equivalent widths of 100–300 mÅ) on the flat part of the curve of growth, and it becomes progressively insignificant with decreasing strengths (i.e., unsaturated weak lines on the linear part) as well as with increasing strengths (i.e., extremely strong damping-dominated lines in the damping part), reflecting the importance of the core-deepening effect caused by the dilution of $S_{\rm L}$ as already mentioned in Sect. 2.2 (cf. Fig. 2).

This naturally explains the behaviors of the extent of the non-LTE corrections for each line at different metallicities and provides the reasons why the weak 6154/6161 lines in disk stars show almost negligible non-LTE effects (cf. Fig. 5c), why the $|\Delta|$ values for the 8183/8195 attain maximum at [Fe/H] ~ -1 (cf. Figs. 5d, 6b, and 7b), and why the $|\Delta|$ value for the 5890/5896 lines systematically decreases from [Fe/H] ~ -2 to ~ -4 (cf. Fig. 7b).

We should note, however, that the situation more or less differs from line to line, each reflecting its individual properties. For example, lines at longer wavelengths tend to suffer larger non-LTE effects because of the decreasing sensitivity of the Planck function to the temperature (i.e., the minimum allowed LTE residual intensity tends to be raised and thus the difference between LTE and non-LTE becomes more significant). Hence, we can understand the fact that

[7] Note that the BAO results are shown only for the 6156/6161 lines in Fig. 7, because those for the other strong lines are comparatively less reliable.

the near-IR 8183/8195 lines show relatively larger non-LTE effects compared to the other lines at similar line-strengths.

Based on Figs. 5–7, we can assess the importance of the non-LTE effect on different lines in sodium abundance determinations as follows: The 6154/6161 lines are the best abundance indicators, for which the non-LTE effect is practically insignificant (i.e., $\lesssim 0.1$ dex) and may be neglected, though they are usable/visible only at $-2 \lesssim$ [Fe/H] $\lesssim +0.4$). The 5683/5688 lines may also be tolerably analyzed with LTE at the metallicity of $-3 \lesssim$ [Fe/H] $\lesssim -1$. Regarding the 5890/5896 and 8183/8195 lines, which are important for diagnosing the Na abundance behaviors of very metal-deficient stars because of their strengths (especially, the 5890/5896 D lines are the only tool for investigating the extremely metal-poor regime of $-4 \lesssim$ [Fe/H] $\lesssim -3$), we consider that properly taking account of the non-LTE effect is necessary.

5.2 Disk Stars

The overall behavior of the Na abundances for disk stars ($-1 \lesssim$ [Fe/H] $\lesssim +0.4$) has long been known to nearly scale with Fe, i.e., [Na/Fe] ~ 0 (e.g., Wallerstein 1962; Tomkin et al. 1985). There seems to be little doubt that this is broadly the case, which finds confirmation also in our Figs. 5–7.[8]

However, our attention is paid rather to the more delicate systematic trend in the [Na/Fe] vs. [Fe/H] relation; namely, the "upturn" revealed by Edvardsson et al.'s (1993) analyses based on the 6154/6161 lines, characterized by slight upward increases on both sides of the broad minimum around [Fe/H] ~ -0.2. Carretta et al.'s (2000) reanalysis of Edvardsson et al.'s (1993) data also reproduced this tendency, as was shown in Fig. 9 of their paper. Similarly, our reanalyzed results on Edvardsson et al.'s (1993) data are essentially the same as their original results (cf. small open circles in Fig. 5c).

Supporting lines of evidence for this trend have been reported from successive analyses on independent observational materials. Feltzing & Gustafsson (1998) confirmed in their Na I 6154/6161 analyses of metal-rich stars that [Na/Fe] progressively increases from ~ 0 ([Fe/H] ~ 0) to $\sim +0.2$ ([Fe/H] $\sim +0.4$) (see the dots in Fig. 5c). They also investigated its behavior in kinematically different stellar groups to see if there is any position-dependent effect in the Galactic chemical evolution, but distinct differences were not observed. Also, Chen et al.'s (2000) LTE analyses of the 6154/6161 lines based on the BAO data of disk stars (common to this study) suggested a weak minimum at [Fe/H] ~ -0.2 superposed on the nearly flat [Na/Fe] (~ 0) (cf. fig. 8 therein), consistent with that found by Edvardsson et al. (1993).

As mentioned in the previous subsection, the non-LTE corrections on the Na I 6154/6161 lines usually used in sodium abundance analyses of disk stars are so small that they are practically negligible. Therefore, it is expected that our non-LTE analyses on these orange lines of multiplet 5 reproduce essentially the same results as obtained by Chen et al. (2000), which expectation is actually confirmed in Fig. 5c. We point out, in addition, that our non-LTE [Na/Fe] values (on the BAO data) derived from other stronger lines (5683/5688, 5890/5896, and 8195) also show signs of the "upturn", (tough not so clear as in the 6154/6161 lines) in spite of their inadequacy for abundance determinations, as can be seen from Figs. 7a, b, and d. Hence, we

[8] Note that Figs. 6–8 include low-gravity giants of population I [e.g., the reanalysis results of Korotin & Mishenina's (1999) data shown by open stars in Fig. 7] showing markedly positive [Na/Fe] values in contrast to others. These stars are expected to have undergone evolution-induced Na enrichment in the envelope due to the dredge-up of Ne-Na cycle products in the H-burning shell, as in the case of supergiants (Takeda & Takada-Hidai 1994). Hence, their abundance characteristics should be distinguishable from those related to the Galactic chemical evolution.

may state that this trend is firmly established.

Considering the decrease of [Na/Fe] with a lowering of [Fe/H] both on the metal-poor side ([Fe/H] $\lesssim -1$; cf. the next subsection) and on the metal-rich side ($0 \lesssim$ [Fe/H]; cf. Feltzing & Gustafsson 1998), the existence of such an "upturn" may indicate an extra production of sodium at the cosmic metallicity of $-1 \lesssim$ [Fe/H] $\lesssim -0.5$. However, any speculation had better be put off until the behaviors of other elements closely related to the synthesis of Na, especially Al and Mg, have been established.

According to our reanalysis results of Prochaska et al.'s (2000) data (cf. diamonds in Fig. 7), the [Na/Fe] values of thick disk stars do not appear to exhibit significantly distinct differences from those of normal thin-disk stars, though our mean non-LTE $\langle$[Na/Fe]$\rangle$ averaged over their 10 stars are nearly zero [$-0.03(\sigma = 0.06)$ and $+0.05(\sigma = 0.04)$ for the 5683/5688 and 6154/6166 lines, respectively] and slightly smaller than the value (0.087) they obtained, which may be due to the non-LTE effect (mean non-LTE corrections are -0.09 and -0.06, respectively).

5.3 Halo Stars

Now, we discuss the behavior of [Na/Fe] for metal-poor halo stars. For simplicity, our discussion is confined to Fig. 7, the results of our reanalysis based on the data taken from the works after 1990, which may presumably be more accurate and reliable than those in Fig. 6 for the reasons mentioned in Sect. 4.3.

One important feature that can be read from Fig. 7 is the systematic decrease of [Na/Fe]; i.e., from [Na/Fe] ~ 0 at [Fe/H] ~ -1 down to [Na/Fe] ~ -0.4 at [Fe/H] ~ -2, though there is a rather large scatter of $\sim \pm 0.2$. This means that we have reasonably reconfirmed the recent results of Baumüller et al. (1998) and Stephens (1999), as opposed to the belief previous to the the mid 1990's (cf. Sect. 1).

It should be stressed that each of the different multiplet lines [5683/5688 (Stephens et al. 1999; half-filled circles), 5890/5896 (McWilliam et al. 1995a; filled circles), 6154/6161 (Kraft et al. 1992; double circles) and 8183/8195 (our OAO data; St. Andrew's crosses)] yielded consistent results with each other, in spite of the considerably different extents of the non-LTE corrections. Thus, we may state that these subsolar [Na/Fe] ratios in metal-poor stars of $-3 \lesssim$ [Fe/H] $\lesssim -1$ are firmly established,[9] while previous LTE analyses using the non-LTE sensitive lines (e.g., McWilliam et al. 1995b, who invoked 5890/5896 lines) must have overestimated the sodium abundances.

Turning our attention to the further extreme metal-poor regime of $-4 \lesssim$ [Fe/H] $\lesssim -3$, we

[9] Some remark may be due regarding our non-LTE reanalysis results of Pilachowski et al.'s (1996) 5890/5896 data (cf. filled triangles in Fig. 7) for population II low-gravity giants mostly having parameter values of $T_{\rm eff} \sim$ 4000–5000 K, $\log g \sim$ 0–2, and $-2.5 \lesssim$ [Fe/H] $\lesssim -1.5$, that do not reveal any such clear subsolar tendency ($\langle$[Na/Fe]$\rangle = 0.00(\pm 0.24)$ on the average) unlike the other cases mentioned above, despite their original LTE results showed a moderate subsolar trend ($\langle$[Na/Fe]$\rangle = -0.17$; cf. Pilachowski et al. 1996). We point out that some of their program stars are low temperature/gravity K giants with parameters $T_{\rm eff} \sim 4000$ K or $\log g \sim 0.0$, which are outside the parameter grid of our non-LTE correction tables and the applied non-LTE correction had to be evaluated by an extrapolation. In these low temperature/gravity cases, it exceptionally happens that the non-LTE effect tends to act as a line-weakening mechanism (i.e., marginally positive non-LTE correction) due to the enhanced $S_{\rm L}$ ($S_{\rm L}/B > 1$) in the line-forming region according to our calculations, as mentioned in footnote 1 in Sect. 2.2. Hence, though appreciable positive non-LTE corrections are actually observed for several stars in Fig. 7b (filled triangles), these are all such low-gravity K giants for which this effect may have been rather erroneously exaggerated by inaccurate extrapolations. Also, because of the temperatures of the Pilachowski et al.'s (1996) program stars are low, the strengths of the 5890/5896 D lines are rather large (200–400 mÅ) in spite of the low metallicity, and comparatively large ambiguities are expected (e.g., equivalent-width measurements, how to choose the damping parameter or the microturbulent velocity). Consequently, our reanalysis results of their data may suffer large uncertainties and should be taken with a grain of salt.

see in Fig. 7 an interesting trend of a rising [Na/Fe] for a lowering of the metallicity, and again a recovering [Na/Fe] ~ 0 at [Fe/H] ~ -4, though the rather insufficient number of stars in this region prevents us from making any definite assertion. It is highly desirable to increase the sample of those stars in order to establish the behavior of [Na/Fe] in this ultra-low metallicity region, which is very important for investigating the history of the early-time Galaxy as well as for constructing a realistic model of Galactic chemical evolution.

Finally, we compare the observed [Na/Fe] vs. [Fe/H] relations obtained for the metal-deficient halo stars with representative theoretical predictions calculated by using various chemical evolution models of our Galaxy. As mentioned in Sect. 1, since the production of Na is dependent on excess neutrons, its yield should naturally be metallicity-dependent and increase with time. As a matter of fact, the assumption of constant yield results in a totally unrealistic [Na/Fe] vs. [Fe/H] relation with a markedly negative d[Na/Fe]/d[Fe/H] gradient (cf. the dashed line labeled "GP(const)" in Figs. 6 and 7, which was taken from fig. 7 of Goswami & Prantzos 2000). It may be possible, therefore, to judge which modeling of Na production (among several proposed chemical evolution calculations) represents the actual situation best by comparing the predicted [Na/Fe] vs. [Fe/H] relation with that observed for halo stars mentioned above. For this purpose, theoretical predictions taken from three recent representative works are depicted in Figs. 6 and 7; namely, those of Timmes et al. (1995; solid lines), Samland (1998; dashed-dotted line), and Goswami & Prantzos (2000; dashed lines). We can draw from Fig. 7 the following conclusions.

— Among these, Timmes et al.'s (1995) results, especially for the case of reduced Fe yield denoted as "TWW (1/2 $\times$)" (cf. Fig. 8a), appear to most satisfactorily reproduce the observed tendency of [Na/Fe] (i.e., the broad/shallow dip-like feature with a minimum around [Fe/H] ~ -2) mentioned above. Their calculations are based on Woosley & Weaver's (1995) yields, simple dynamical model for the Galaxy with infall, a standard Salpeter (1955) initial-mass function (IMF) and a quadratic Schmidt star-formation rate. (Each line corresponds to the different choice of the Fe yield from massive stars; i.e., that from the original Woosley & Weaver paper and that reduced by a factor of 2; the latter is rather recommended by Timmes et al. 1995).

— Samland's (1998) model is based also on Woosley & Weaver's (1995) yields. However, since he adjusted the metallicity-dependent Na yield in his own way [cf. equation (9) therein] so as to fit the observed trend of [Na/Fe] known at the time of mid-1990's (i.e., erroneously overestimated to be [Na/Fe]~ 0 even for halo stars), his prediction does not fit the observed [Na/Fe] obtained in this study.

— Goswami & Prantzos's (2000) calculation (labeled "GP(var)"in Fig. 7) explains the decline of [Na/Fe] from [Fe/H]~ -1 to [Fe/H]~ -2 reasonably well. However, their prediction suggests an ever-decreasing (or a plateau-like) [Na/Fe] toward the extremely low metallicity regime ([Na/Fe]~ -4), which apparently contradicts the tendency we found. While their model is based on Woosley & Weaver's (1995) metallicity-dependent yields (as was done by Timmes et al. 1995) with a Fe yield reduced by a factor of 2, they used a different IMF (Kroupa et al. 1993) and a different halo model. From this point of view, the dynamical model of the Galaxy and IMF adopted by Timmes et al. (1995) might be preferable to those of Goswami & Prantzos (2000), as far as the early Galaxy ([Fe/H] $\lesssim -2$) is concerned.

6 CONCLUSION

We carried out extensive non-LTE calculations on the atomic model of neutral sodium and model atmospheres with a wide range of parameters, for the purpose of non-LTE abundance determinations based on eight representative Na I lines at 5683, 5688, 5890, 5896, 6154, 6161, 8183, and 8195 Å.

The non-LTE effect almost always acts as a line-strengthening mechanism (hence making the non-LTE abundance correction negative). Though its extent differs from line to line (from almost negligible level of a few hundredths dex to a considerable amount of ~ 0.5 dex), strong saturated lines (though not too strong to be damping-dominated) tend to suffer a large non-LTE effect. Generally speaking, the lines for which non-LTE corrections had better be taken into account in Na abundance determinations are the 5890/5896 and 8183/8195 lines, while the 5683/5688 and (especially) 6154/6161 lines are comparatively less sensitive to the non-LTE effect.

Our non-LTE reanalysis of our BAO and OAO equivalent-width data along with those taken from extensive literature led to the following conclusions:
— (1) Regarding the disk stars with $-1 \lesssim$ [Fe/H] $\lesssim +0.4$, we confirmed the existence of a delicate "upturn" feature (i.e., a broad/shallow dip around the minimum at [Fe/H] ~ -0.2) superposed on the general tendency of [Na/Fe] ~ 0, as has been reported by recent analyses on weak Na I 6154/6161 lines being inert to any non-LTE effect. Moreover, according to our analyses on our BAO data, even the abundances derived from strong (saturated or damping-dominated) lines, which are generally unsuitable for abundance analyses, suggested this tendency.
— (2) We found from our analyses of recent data after 1990's that the [Na/Fe] ratios for metal-poor halo stars show a "subsolar" behavior; i.e., [Na/Fe] decreases from ~ 0 (at [Fe/H]~ -1) to ~ -0.4 (at [Fe/H]~ -2), and that, with a further decrease in metallicity, it appears to rise again to ~ 0 at [Fe/H]~ -4. It is evident that the previous suggestion of almost solar Na-to-Fe ratio over all metallicity, which was actually believed until mid 1990's, is attributed to the overestimation of sodium abundances due to the neglect of the non-LTE effects. Among the representative theoretical models of Galactic chemical evolution, that of Timmes et al. (1995) appears to reasonably reproduce this behavior.
— (3) Given this piece of observational evidence, the run of [Na/Fe] is in rough accord with that of [Al/Fe] (cf. Baumüller & Gehren 1997), which would be reasonable from a theoretical point of view, since both are expected to show similar behaviors (see, e.g., sect. 5.8 of Samland 1998). In order to further clarify the connection between the present results and the abundances of such important Na-related elements in metal-poor stars, we are now planning to carry out extensive non-LTE analyses on Al and Mg, in the way similar to that adopted in this paper by using our own as well as the other published data, and we will report the results in our forthcoming papers.

Acknowledgements We thank the staff members of OAO, especially H. Izumiura and S. Masuda, for their kind support and suggestions concerning the operation and maintenance of HIDES. Thanks are also due to S. Honda, K. Sadakane, S. Sato, and K. Osada for their helpful collaborations in our 2001–2002 observations at OAO. This work was done within the framework of the China–Japan collaboration project, "Galactic Chemical Evolution through Spectroscopic Analyses of Metal-Deficient Stars" supported by the Japan Society for the Promotion of Science (JSPS) and the National Natural Science Foundation of China (NSFC).

References

Allende Prieto C., Asplund M., García López R. J. et al., 2002, ApJ, 567, 544
Alonso A., Arribas S., Martínes-Roger C., 1999, A&AS, 139, 335
Anders E., Grevesse N., 1989, Geochim. Cosmochim. Acta, 53, 197
Baumüller D., Butler K., Gehren T., 1998, A&A, 338, 637
Baumüller D., Gehren T., 1997, A&A, 325, 1088
Beckers J. M., Bridges C. A., Gilliam L. B., 1976, AFGL Tech. Rept., No. 76-0126
Beveridge C. R., Sneden C., 1994, ApJ, 108, 285
Carretta E., Gratton R. G., Sneden C., 2000, A&A, 356, 238
Chen Y. Q., Nissen P. E., Zhao G. et al., 2000, A&AS, 141, 491
Edvardsson B., Andersen J., Gustafsson B. et al., 1993, A&A, 275, 101
Feltzing S., Gustafsson B., 1998, A&AS, 129, 237
François P., 1986a, A&A, 160, 264
François P., 1986b, A&A, 165, 183
Fulbright J. P., 2000, AJ, 120, 1841
Goswami A., Prantzos N., 2000, A&A, 359, 191
Gratton R. G., Carretta E., Eriksson K. et al., 1999, A&A, 350, 955
Gratton R. G., Sneden C., 1987a, A&A, 178, 179
Gratton R. G., Sneden C., 1987b, A&AS, 68, 193
Gratton R. G., Sneden C., 1988, A&A, 204, 193
Gratton R. G., Sneden C., 1994, A&A, 287, 927
Holweger H., 1971, A&A, 10, 128
Korotin S. A., Mishenina T. V., 1999, Astron. Rep., 43, 533
Kraft R. P., Sneden C., Langer G. E. et al., 1992, AJ, 104, 645
Kroupa P., Tout C. A., Gilmore G., 1993, MNRAS, 262, 545
Kurucz R. L., 1979, ApJS, 40, 1
Kurucz R. L., 1993a, Kurucz CD-ROM, No. 13, Harvard-Smithsonian Center for Astrophysics
Kurucz R. L., 1993b, Kurucz CD-ROM, No. 14, Harvard-Smithsonian Center for Astrophysics
Kurucz R. L., Furenlid I., Brault J. et al., 1984, Solar Flux Atlas from 296 to 1300 nm, Sunspot, New Mexico: National Solar Observatory
Lambert D. L., Luck R. E., 1978, MNRAS, 183, 79
Luck R. E., Bond H. E., 1985, ApJ, 292, 559
Magain P., 1989, A&A, 209, 211
Mashonkina L. I., Shimanskǐ V. V., Sakhibullin N. A., 2000, Astron. Rep., 44, 790
McWilliam A., Preston G. W., Sneden C. et al., 1995a, AJ, 109, 2736
McWilliam A., Preston G. W., Sneden C. et al., 1995b, AJ, 109, 2757
Molaro P., Bonifacio P., 1990, A&A, 236, L5
Nissen P. E., Primas F., Asplund M. et al., 2002, A&A, 390, 235
Peterson R. C., 1980, ApJ, 235, 491
Peterson R. C., 1981, ApJS, 45, 421
Peterson R. C., 1989, ApJ, 347, 266
Peterson R. C., Carney B. W., 1979, ApJ, 231, 762
Peterson R. C., Kurucz R. L., Carney B. W., 1990, ApJ, 350, 173
Pilachowski C. A., Sneden C., Kraft R. P., 1996, ApJ, 111, 1689
Primas F., Molaro P., Castelli F., 1994, A&A, 290, 885
Prochaska J. X., Naumov S. O., Carney B. W. et al., 2000, AJ, 120, 2513
Sadakane K., Ohkubo M., Takeda Y. et al., 2002, PASJ, 54, 911

Salpeter E. E., 1955, ApJ, 121, 161
Samland M., 1998, ApJ, 496, 155
Steenbock W., Holweger H., 1984, A&A, 130, 319
Stephens A., 1999, AJ, 117, 1771
Stürenburg S., Holweger H., 1990, A&A, 237, 125
Takada-Hidai M., Takeda Y., Sato S. et al., 2002, ApJ, 573, 614
Takeda Y., 1991, A&A, 242, 455
Takeda Y., 1995, PASJ, 47, 463
Takeda Y., Takada-Hidai M., 1994, PASJ, 46, 395
Takeda Y., Zhao G., Chen Y.-Q. et al., 2002, PASJ, 54, 275
Timmes F. X., Woosley S. E., Weaver T. A., 1995, ApJS, 98, 617
Tomkin J., Lambert D. L., Balachandran S., 1985, ApJ, 290, 289
Unsöld A., 1955, Physik der Sternatmosphären, 2nd ed., Berlin: Springer, p.333
Wallerstein G., 1962, ApJS, 6, 407
Wiese W. L., Smith M. W., Miles B. M., 1969, Atomic Transition Probabilities Vol.II — Sodium Through Calcium, NSRDS-NBS22, Washington, DC: US Government Printing Office
Woosely S. E., Weaver T. A., 1995, ApJS, 101, 181
Zhao G., Magain P., 1990a, A&A, 238, 242
Zhao G., Magain P., 1990b, A&AS, 86, 85